Appl. Phys. B (2015) 118:517–525
DOI 10.1007/s00340-015-6018-z

Applied Physics B
Lasers and Optics

Spectroscopy and laser cooling on the $^1S_0$–$^3P_1$ line in Yb via an injection-locked diode laser at 1,111.6 nm

Injection locking for the yellow–green spectrum

N. Kostylev · C. R. Locke · M. E. Tobar · J. J. McFerran

Received: 25 November 2014 / Accepted: 20 January 2015 / Published online: 10 February 2015

Abstract We generate 555.8-nm light with sub-MHz linewidth through the use of laser injection locking of a semiconductor diode at 1,111.6 nm, followed by frequency doubling in a resonant cavity. The integrity of the injection lock is investigated by studying an offset beat signal between slave and master lasers, by performing spectroscopy on the $(6s)^2\ ^1S_0$–$(6s6p)\ ^3P_1$ transition in magneto-optically trapped ytterbium, and by demonstrating additional laser cooling of ^{171}Yb with the 555.8-nm light in a dual-wavelength magneto-optical trap (MOT). For the $^1S_0$–$^3P_1$ spectroscopy, we confirm the linear dependence between ground-state linewidth and the intensity of an off-resonant laser, namely that used to cool Yb atoms in a $^1S_0$–$^1P_1$ magneto-optical trap. A temperature of 60 μK is produced for ^{171}Yb in the dual-wavelength MOT. Our results demonstrate the suitability of injection-locked 1,100–1,130-nm laser diodes as a source for sub-MHz linewidth radiation in the yellow–green spectrum.

1 Introduction

Generating narrow-linewidth laser sources in the visible spectrum is a common objective, particularly in the field of atomic and molecular spectroscopy. In this work, we focus attention on low-noise light generation at 555.8 nm needed for laser cooling of ytterbium, though the scheme can be employed for wavelengths nearby; for example, those used in an iodine frequency reference [1–3] or in confocal laser scanning microscopy [4]. Laser cooling of ytterbium is becoming more prevalent as the range of atomic studies and applications increase. Optical lattice clocks based on ytterbium have achieved significant milestones [5, 6], which has led to the rapid development of Yb lattice clocks at a number of institutions [7–10]. Since the early magneto-optical trapping of Yb [11], a range of cold atoms experiments have been performed producing Bose–Einstein condensation [12, 13], multi-species magneto-optical trapping with Yb [14–16], photo-association spectroscopy of excited heteronuclear Yb molecules [17], and quantum degenerate mixtures involving Yb [18–21]. Ytterbium is used to study ultra-cold phenomena in SU(N) systems [22–24] and the related study of topological phases [25, 26]. Investigations have been carried out studying sub-radiance in lattice bound Yb_2 molecules [27]. Furthermore, cold ytterbium atoms or hetero-nuclear Yb molecules are good candidates in the search for a permanent electric-dipole moment [28, 29] and studying quantum magnetism [30].

While methods do exist for generating low-noise 555.8-nm laser light, they are generally cost disadvantageous in comparison with diode laser systems. Furthermore, crystal waveguides (e.g., based on lithium niobate) that are often used for efficient frequency doubling have been known to suffer degradation in conversion efficiency over months or years [31, 32]. The technique here uses a low-power fiber laser at 1,111.6 nm, and then through optical injection of a semiconductor diode laser, the available power is increased while maintaining the low noise characteristic of the fiber laser. To confirm that the narrow linewidth of the source laser is transferred to the slave laser, we perform spectroscopy on the $^1S_0$–$^3P_1$ line in magneto-optically trapped ytterbium, where cooling and trapping of ^{172}Yb is carried out using the $^1S_0$–$^1P_1$ transition. Conversion to 555.8-nm is performed with a single pass through a periodically poled potassium titanyl phosphate crystal. We deduce that the linewidth contribution

N. Kostylev · C. R. Locke · M. E. Tobar · J. J. McFerran (✉)
School of Physics, University of Western Australia,
Crawley 6009, Australia
e-mail: john.mcferran@uwa.edu.au

from the 555.8-nm light is below 410 ± 90 kHz. The level of 555.8-nm light is then enhanced in a resonant frequency doubling cavity. This is used in a dual wavelength magneto-optical trap involving the $^1S_0$–$^1P_1$ (398.9 nm) and $^1S_0$–$^3P_1$ (555.8 nm) lines. We show sub-100 μK temperatures for ^{172}Yb, verifying the low noise properties of the green light. To our knowledge, this is the first report of the use of optical injection-locking of ridge-waveguide diode lasers for narrow-linewidth green light emission near 556 nm. A related method has been used for 578-nm yellow light generation [33], but there the master laser was an extended cavity diode laser locked to a high-finesse optical cavity and a distributed feedback laser was injection locked, making for a more complicated setup (following the need to probe the much narrower Yb $^1S_0$–$^3P_1$ transition). Single-mode diode lasers in the 1,100–1,130-nm range still remain scarce: we demonstrate one of few instances, and perhaps the first, of using them in atomic spectroscopy.

2 Laser injection locking at 1,111.6 nm

The generation of sufficient power of 555.8-nm light is often achieved by amplifying the output of a Yb-doped fiber laser with a Yb fiber amplifier and then frequency doubling in a periodically poled lithium niobate crystal or waveguide [4, 34–36]. Here we demonstrate a cost-effective method that also relies on a Yb fiber laser as a master laser, but amplification is by way of injection locking a semiconductor laser followed by a resonant frequency doubling stage. The master laser is a fiber laser producing 6 mW of light with a specified linewidth of less than 60 kHz. The slave laser is a ridge-waveguide semiconductor laser (Eagleyard, EYP-RWL-1120) with a central wavelength of 1,110 nm and a maximum power of 50 mW. The injection-locking scheme is outlined in Fig. 1, where light from the fiber laser is directed into the semiconductor laser using the rejection port of an optical isolator.

As a first means of testing the quality of the injection lock, 120 μW of the master laser light is frequency shifted with an acousto-optic modulator (AOM) and heterodyned with 110 μW of the slave laser light. The resultant beat signal, at 90 MHz, exhibits a signal-to-noise ratio (SNR) of ∼70 dB (3-kHz resolution bandwidth) when 3 mW of master laser light is coupled into the slave laser. An example of the field spectrum is shown in Fig. 2a. The linewidth of the optical beat signal is given mostly by that of the voltage-controlled oscillator driving the AOM (measured to be ∼3 kHz at 1-kHz resolution bandwidth and 300 ms of sweep time). Its noise is not imposed on the semiconductor laser since the AOM is not in the path of the injecting light leading to the slave laser. The presence alone of the beat signal is an indication of injection locking occurring because the diode laser is not tuneable to

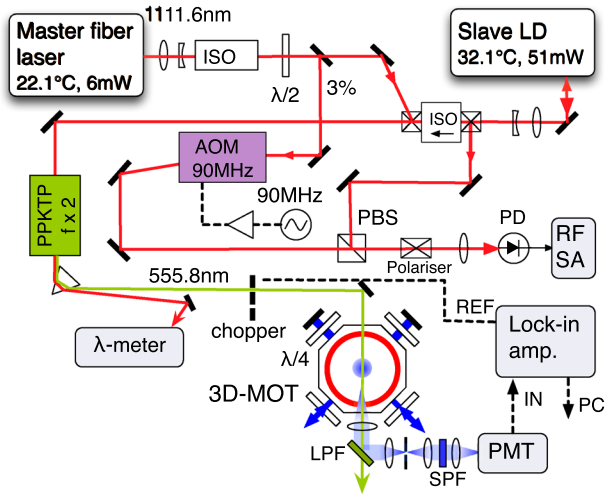

Fig. 1 Experimental setup for the $^1S_0$–$^3P_1$ spectroscopy of ^{172}Yb atoms in a $^1S_0$–$^1P_1$ magneto-optical trap. A narrow linewidth (∼60 kHz) fiber laser injection locks a semiconductor laser to increase the available power. A few percent of the injecting light is frequency offset with an acousto-optic modulator ($f = 90$ MHz) and heterodyned with the slave laser light to monitor the quality of the injection lock. The diode laser light is frequency doubled using a periodically poled potassium titanyl phosphate (PPKTP) crystal. This *green laser light* is modulated with a rotating chopper. Fluorescence from the cold atoms de-exciting from the $^1P_1$ state is detected by a photomultiplier cell (PMT), and the modulation on the fluorescence is detected with a lock-in amplifier referenced to the chopper frequency to recover the spectroscopic signal. *ISO* optical isolator, *LD* laser diode, *LPF* long-pass filter at 505 nm, *MOT* magneto-optical trap, *PBS* polarizing beam splitter, *SA* spectrum analyzer, *SPF* short-pass filter at 500 nm)

the wavelength of 1,111.6 nm (the nearest wavelength that the diode laser could be tuned was 1,111.53 nm after an exploration across temperature and diode current). Furthermore, a beat signal between the lasers without injection locking produces a linewidth of approximately 20 MHz—that of the free running semiconductor laser (details below). The residual bumps either side of the beat signal in Fig. 2a may be due to a relaxation oscillation in the fiber laser, since the sideband frequency matches that at which there is a peak in the relative intensity noise of the fiber laser. At −70 dB below the carrier, it is not a significant concern.

A demonstration of the change in wavelength of the slave laser under the influence of the master laser is seen in Fig. 2b. Here the shift in frequency is 240 GHz, showing the extent of the locking range. This locking range is observed for injected light power above 150 μW. Only at much higher resolution are the frequency excursions seen, for example, as shown in the inset. The quality of the injection lock is discerned using the signal strength of the optical beat note. In Fig. 3a, we show the beat signal strength versus the optical power of the injected light. The beat strength increases with a power-law dependence on

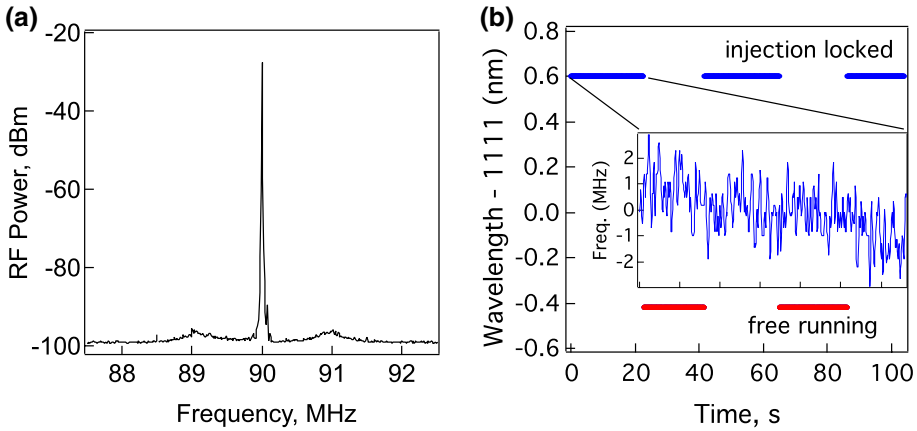

Fig. 2 **a** An optical beat signal between the slave diode laser and the AOM-shifted master laser with 3-kHz resolution bandwidth. **b** Illustrating the wavelength shift of the diode laser by injection of light from the master laser. The 1-nm locking range corresponds to 240 GHz. *Inset*: The slave laser frequency, offset by the carrier frequency

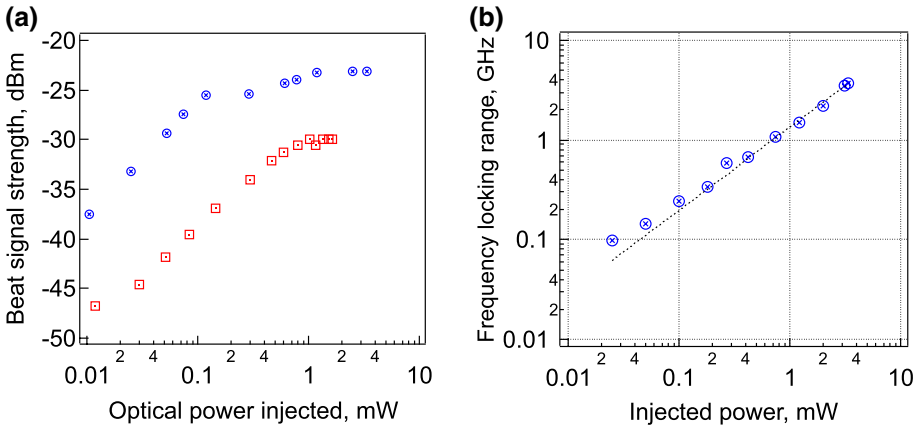

Fig. 3 **a** Variation of the beat signal strength between slave and master lasers (offset by an AOM) versus the optical power of the injected light. Two examples are shown where the quality of the mode matching differs, with the upper trace having improved mode matching. **b** Frequency locking range versus the optical power of the injection-locking light

the injected light power until a saturation level is reached, which depends on the quality of the mode coupling into the slave laser. In the case of optimized mode coupling (hollow circles), the saturation power occurs at about 100 μW. The lower trace (hollow squares) shows an example where the mode coupling is not optimized, but the power-law dependence is more evident. Another power-law dependence is seen between the frequency tuning range (or locking range [37]) of the slave laser and the injected light power, P, as shown in Fig. 3b. The measurement is taken by adjusting a piezoelement in the master laser, and we choose the locking range as the range of frequencies over which the SNR of the offset beat remains above 40 dB (resolution bandwidth = 10 kHz). There is a sharp rise in amplitude noise at the extents of the locking range, making for a clear demarcation. We note that the power law does not exhibit the square-root dependence sometimes seen for the locking range versus intensity, but rather a $\sim P^{0.8}$ dependence. There may be a beam spot-size dependence on power, thereby affecting the intensity.

The linewidth of the free running semiconductor laser was measured by generating an optical beat signal between the fiber laser and the free running diode laser, without the injection locking. Adjustments were made to the slave laser diode temperature and current, and to the fiber laser temperature to tune the frequencies sufficiently close to one another for heterodyne detection on a photodetector. In this case, the wavelength was 1,111.46 nm. The optical beat exhibited a linewidth of ∼18 MHz, where we can safely assume that the majority of the noise is due to the diode laser. Where this light to be frequency doubled to 555.8 nm, the corresponding linewidth would be approximately 70 MHz. This may be compared with the much narrower $^1S_0$–$^3P_1$ spectra obtained below. In demonstrating the versatility of the 1110-nm diode lasers, a second semiconductor laser chip was placed in an extended cavity with a diffraction grating (1200 grooves mm^{-1}) acting as the frequency selecting element. This laser was heterodyned separately with the master fiber laser producing an optical beat note with a linewidth of 600 kHz (sweep time of 20 ms).

3 Spectroscopy of the $^1S_0$–$^3P_1$ line in laser-cooled Yb

An unequivocal way of determining the resultant linewidth of the injection-locked laser is to set up two independent

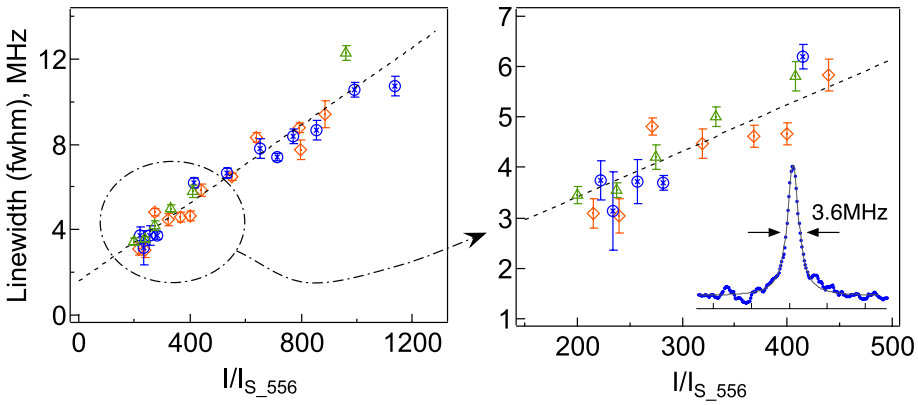

Fig. 4 The full-width half-maxima of $^1S_0$–$^3P_1$ ^{172}Yb spectra versus the six-beam intensity in the $^1S_0$–$^1P_1$ magneto-optical trap. The intensity is normalized using the $^1S_0$–$^3P_1$ saturation intensity of 1.4 W m^{-2}. The *different markers* represent data recorded on separate days. All data contribute to the line fit. *Inset*: $^1S_0$–$^3P_1$ spectrum of the magneto-optically trapped ^{172}Yb atoms for a 398.9-nm cooling laser intensity of 390 W m^{-2} ($280I_{S\_556}$)

master and slave laser systems and produce a heterodyne beat. Without access to a second fiber laser, we instead perform $^1S_0$–$^3P_1$ spectroscopy on cold ytterbium atoms to verify the noise properties of the slave laser. Here we use ^{172}Yb atoms confined in a magneto-optical trap (MOT) that makes use of the 398.9 nm $^1S_0$–$^1P_1$ transition. The temperature of the ^{172}Yb and ^{174}Yb atoms (composite bosons) in the MOT has previously been shown to be approximately 1.1 mK [38]. The corresponding Doppler width, based on the expression $\Delta\nu_D = \nu[8\ln(2)k_BT/mc^2]^{1/2}$, is ~1.0 MHz when probing the atoms with 555.8-nm light. Here, ν is the $^1S_0$–$^3P_1$ frequency, k_B is the Boltzmann constant, T is temperature, and m is the mass of ^{172}Yb. The spectroscopy is performed while the MOT fields are held constant, and therefore, the $^1S_0$–$^3P_1$ is influenced by ground-state broadening from the cooling light (sometimes referred to as Rabi broadening [39]). We choose ^{172}Yb due to the simpler energy-level structure compared with the fermonic isotopes. No DC magnetic field is applied to split the m_J levels as the magneto-optical trap ensures that the B-field is at (or close to) zero field at the location of the atoms (we safely state this because the $m_{J=0} \rightarrow m_{J=\pm1}$ *side lobes* observed in the work of Loftus et. al. [40] are mostly unobservable or unresolvable). However, the linear polarization of the 555.8-nm light is set parallel to that of the B-field of the Zeeman slower to minimize any influence from the Zeeman slower field.[1]

The slave laser light is frequency doubled using a periodically poled potassium titanyl phosphate (PPKTP) crystal in a single pass, producing ~3.5 μW of 555.8-nm light with 36 mW of fundamental light incident. The poling period is 10.275 μm (Raicol Crystals specification) and the crystal temperature for optimum frequency doubling is 55.7 °C (the FWHM temperature bandwidth is 3.5 °C). The 555.8-nm probe beam, with 2.4 μW of optical power sent to the MOT chamber, is modulated with a chopper wheel rotating at 379 Hz. The probe creates a depletion in the ground state and a corresponding modulation is produced in the 398.9-nm fluorescence of the cold atoms. The fluorescence is detected with a photomultiplier cell (Hamamatsu 10492-001, 1 V/μA, bandwidth of 20 kHz) and the modulation is down-converted with a lock-in amplifier that is referenced to the chopper wheel frequency. A short-wavelength pass filter with an optical density of 6.0 at 556 nm prevents any stray green light reaching the photomultiplier cell. The 398.9-nm light was intensity stabilized via an amplitude modulation servo that uses the same AOM that controls the violet light's frequency detuning. The technique differs from previous $^1S_0$–$^3P_1$ spectroscopy in a ytterbium MOT, where 556-nm fluorescence was detected and the measurements were recorded at DC [39, 40]. An example of the spectra obtained here is shown in the inset of Fig. 4, in this case, with a MOT light field intensity of 390 W m^{-2}. The frequency scale is determined with the aid of a wavemeter that continually records the wavelength of the 1,111.6-nm light (and the frequency doubling is taken into account). A piezoelement in the fiber laser permits scanning of the laser frequency. The time taken to sweep across the FWHM of the resonance is ~4 s, and the maximum drift rate of the master laser is 2.1 kHz s^{-1} (4.2 kHz s^{-1} at 556 nm); therefore, the drift does not strongly influence the spectral width of the lines. Any influence is reduced by scanning in alternate directions across the transition and calculating a mean FWHM. The dependence of the spectral width of the $^1S_0$–$^3P_1$ line as a function of the optical intensity in the MOT is shown in Fig. 4. The intensity is normalized by the saturation intensity of the $^1S_0$–$^3P_1$ transition; i.e., $I_{S\_556} = 1.4$ W m^{-2} (the relevant saturation intensity here is that of the probe rather than the trapping field, despite the latter being the parameter that is varied). The different markers represent data recorded on separate days. Each data point is the weighted mean of between three and five measurements, where each

[1] With the 555.8-nm light polarized orthogonally to the Zeeman slower B-field we observe splitting of the $^3P_1$ sub-states and so can verify the B-field strength of the Zeeman slower.

measurement is the mean FWHM of typically four line scans. The Zeeman slower beam intensity was reduced to $\sim 0.3\, I_{S\_399}$ (or 120 I_{S_556}) for these measurements; however, the $^1S_0$–$^3P_1$ linewidth was found to be independent of the Zeeman beam intensity and so is not included in the intensity values of Fig. 4 (its detuning was $-7.0\ \Gamma_{399}$, where Γ_{399} is the natural linewidth of the $^1S_0$–$^1P_1$ transition). There is a clear reduction in linewidth in Fig. 4 as the intensity is reduced. The relationship often used to describe intensity broadening is $\Delta\omega(I) = \Gamma(1 + I/I_S)^{1/2}$, where Γ is the natural linewidth, or more generally, the homogenous linewidth in the absence of light [41, 42]. However, here the experiment is arranged such that only the ground state of the $^1S_0$–$^3P_1$ transition is affected by strong intensity perturbations, and line broadening of the ground state is characterized by a linear dependence on intensity [39, 43]. The 556-nm light intensity was $\approx 0.012\ I_{S\_556}$, so its contribution to line broadening is negligible. Along with the natural linewidth, there are also other contributions to the zero-intensity linewidth; for example, the inhomogeneous broadening from the residual velocity of the cold atoms ($\Delta\nu_D$), and noise from the 555.8-nm light ($\Delta\nu_L$). Incorporating these into the expression for spectral width, we have $\Delta\nu_m(I) \approx \Delta\nu_D + \Delta\nu_L + (\Gamma/2\pi)(1 + bI/I_{S\_556})$, where b characterizes the slope. The dashed line of Fig. 4 shows the weighted line fit to all of the data, producing an ordinate intercept of 1.59 ± 0.09 MHz. The product-moment correlation coefficient (Pearson's r coefficient) is 0.89, supporting the linear relationship between the linewidth and the intensity. Subtracting linewidth contributions due to Doppler broadening ($\Delta\nu_D = 1.0$ MHz) and the natural linewidth ($\Gamma_{556} = 182$ kHz) leaves a contribution from the 555.8-nm light of $\Delta\nu_L \approx 410 \pm 90$kHz. The 1,111.6-nm fiber laser has a linewidth specification of 60 kHz; therefore, the linewidth at 555.8 nm should be about 240 kHz (making the tenable assumption that the laser noise is dominated by white frequency noise). Our measurement is reasonably consistent with this estimate. In fact, it should be treated as an upper bound on the laser's linewidth since residual $m_{J=0} \rightarrow m_{J=\pm1}$ splitting may to contribute to the linewidth if the atom cloud is offset from the MOT center (and this is more likely to occur when the MOT light fields are weak). We note that the temperature of the Yb atoms increases with the cooling laser intensity; therefore, the Doppler broadening contribution to the linewidth will also increase. However, here the corresponding maximum linewidth (at $\sim 1{,}200 I_{S\_556}$) is only ~ 1.6 MHz based on Doppler cooling theory (at a frequency detuning equal to 1.5 times the linewidth of the $^1S_0$–$^1P_1$ transition). Thus, the contribution to the linewidths in Fig. 4 from this effect is small (and, moreover, has a $I^{1/2}$ dependence). Although we did not detect it, one may expect some ground-state broadening from the Zeeman slower beam, which would also lead to an overestimate of the laser linewidth (despite the slowing beam's frequency detuning being $-7\ \Gamma_{399}$, this should still cause some perturbation to the $^1S_0$ state). Reduced uncertainty on the zero-intensity spectral width would be achieved if the 398.9-nm laser cooling light could be reduced further. However, below 200 I_{S_556} ($\sim 300\, W\,m^{-2}$ or 0.5 I_{S_399}), there is insufficient cooling intensity to trap adequate numbers of atoms in the MOT for $^1S_0$–$^3P_1$ line detection.

Another test regarding the injection locking is to reduce the power of the light injected into the slave laser diode and to observe whether there is an influence on the width of the $^1S_0$–$^3P_1$ spectral line when probing the cold atoms. We found that there was no noticeable change in the spectral width versus injected power and that only the strength of the spectroscopic signal weakens as the injected power is reduced. The control bandwidth of the injection locking is therefore well beyond the range of several MHz as one might expect [44]. The change in strength of the $^1S_0$–$^3P_1$ signal with injected power implies that the fraction of slave laser light that is coherent with the master laser also changes with injected power. Below a threshold of about 1 mW, the fraction of slave laser light that is coherent with the master laser light reduces with a logarithmic dependence, in our case with a slope of $\approx 0.05\ \mathrm{dBm}^{-1}$.

4 Magneto-optical trapping with 555.8-nm light

To enhance the power level of 555.8-nm light, the PPKTP crystal has been placed in a resonant frequency doubling cavity [45]. The cavity is designed to generate a 35 μm waist at the crystal location in both vertical and horizontal planes. The radius of curvature of the folding mirrors is 75 mm, and full length of the cavity is 568 mm. The cavity resonances further demonstrate the effectiveness of the injection locking, since clear Lorenztian lineshapes are resolved by the cavity. Without injection locking, the resonances are heavily obscured. The cavity is readily locked to the center of resonance with the frequency modulation method ($f_{\mathrm{mod}} = 33$ kHz). We confer a 4.5 kHz servo bandwidth between the second-harmonic generating cavity and the 1,111.6-nm light (which may be restricted by the phase roll-off produced by the lock-in amplifier used to generate the error signal).

The beam profile of the 1111.6-nm diode laser light is adjusted with two pairs of cylindrical lenses for improved coupling into a single-mode optical fiber. The fiber spatially filters the light to aid with the mode matching into the frequency doubling cavity and transports the light to the magneto-optical trap table. Through the fiber, 52 % of the light passes, making available 24 mW for the resonant cavity (there is some irregular, non-Gaussian, structure

in the semiconductor beam profile, hence the lower than usual coupling). The spherical Gaussian beam profile out of the fiber helps to achieve 98.5 % mode matching into the TEM00 mode of the second-harmonic generating cavity. By observing the reflection from the input coupler, the fraction of the 1,111.6-nm light coupled into the cavity is, at most, 58 %. We see increased coupling as the incident power increases. It follows that the impedance matching improves as the nonlinear conversion increases. The optimum reflectivity of the input coupler can be approximated using $R_{\mathrm{opt}} \approx 1 - P_c\gamma - \epsilon$, where P_c is the circulating power, γ is the single-pass nonlinear conversion efficiency ($0.026\,\mathrm{W}^{-1}$) [46], and ϵ represents other losses of fundamental power in the cavity excluding that at the input coupler [46, 47]. It is evident in our case that ϵ is very low because the finesse of the cavity corresponds closely to the losses produced by the transmission of the input coupler ($R = 0.93$). Making up the difference, we find $\epsilon \sim 0.01$. The power enhancement is about 28; hence, for an input power of 25 mW, the optimum input coupler reflectivity is ~0.96 (the power enhancement varies by ~14 % over $0.93 < R < 0.99$). Should diode lasers at 1110 nm become available with higher power, the impedance matching condition will be better met. Alternatively, if an input coupler with $R = 0.96$ is used, an increase of about 30 % in the level of 555.8-nm light may be obtained. We can readily produce 8 mW of 555.8-nm light—when half of this light is incident upon the atoms in the $^1S_0$–$^1P_1$ MOT, the atoms are completely ejected from the trap. Moreover, for a beam with an e^{-2} radius of 5 mm, a power level of 8 mW corresponds to an intensity 150 times the saturation intensity of the $^1S_0$–$^3P_1$ transition.

To confirm the narrow linewidth of the 555.8-nm light, we have tested its suitability for laser cooling of Yb, where we have implemented a dual-stage magneto-optical trap using dichroic filters to combine the 398.9-nm and 555.8-nm beams, and achromatic quarter wave plates for the polarization control. The arrangement is outlined in Fig. 5. The overlapping beam paths at the two wavelengths produces a compact configuration and eases the alignment process for the 555.8-nm light. The photo-multiplier tube of Fig. 1 is now replaced with a CCD camera to image the cloud of atoms. The green light frequency is stabilized using an frequency modulation servo on the Yb thermal beam before the Zeeman slower. The servo bandwidth is approximately 5 Hz. Locking to a 37 MHz wide line with a signal-to-noise ratio of ~160 in 3 s (for ^{171}Yb) produces a stability at 1 s comparable to that of Γ_{556}. The 555.8-nm beam radius (e^{-2}) for the MOT is ~2.6 mm. The narrow diameter of the beams is afforded by the action of the first-stage MOT.

Figure 6a shows the enhancement of the cold atoms' fluorescence when the 555.8-nm light is red-detuned with

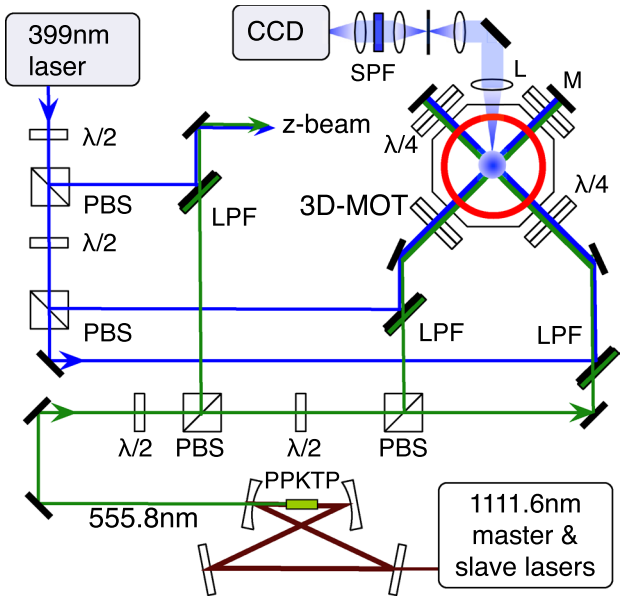

Fig. 5 Sketch of the setup for the dual $^1S_0$–$^1P_1$ and $^1S_0$–$^3P_1$ magneto-optical trap (MOT). The 398.9-nm and 555.8-nm beams proceed along the same paths through the MOT. Not shown are the frequency stabilization schemes for the 398.9-nm and 555.8-nm light, nor the frequency doubling method used to generate the 398.9-nm light. *CCD* charged coupled device, *L* lens, *LPF* long-pass filter at 505 nm, *M* mirror, *PBS* polarizing beam splitter, *PPKTP* periodically poled potassium titanyl phosphate, $\lambda/4$ dual wavelength (399 and 556 nm) quarter wave plate, *SPF* short-pass filter at 505 nm; z-beam, refers to the beam along the *strong* axis of the MOT

respect to the $^1S_0$–$^3P_1$ transition. The fluorescence was recorded 2.5 ms after the ^{171}Yb atoms were released from the 398.9-nm light and magnetic field gradient. The 398.9-nm light was ramped down to zero intensity over 10-ms before the release (and is re-instituted for the fluorescence detection). The cycle time and therefore time taken between data points is 1 s, and the plot was produced by averaging over six scans. The two sets of markers represent forward and reverse sweeps across the transition. While the relative frequency scale is well calibrated, the absolute frequency with respect to the line center is not, but it is coarsely estimated from the known characteristics of laser cooling. The asymmetric line shape is characteristic of spectra obtained with magneto-optical traps—the sharp roll-off near resonance reflecting the sudden transition from trapping to dispersing the atoms. The linewidth is approximately 1.6 MHz, or about $9\,\Gamma_{556}$, demonstrating the capture range in terms of frequency detuning ($I \sim 240\,I_{S\_556}$).

In Fig. 6b, we show two traces representing the free expansion of the atom cloud; that is, the rms cloud radius versus the free expansion time (using squared values to show the linear relationship). The upper trace is that for ^{171}Yb atoms in the 398.9-nm MOT; both the 398.9-nm

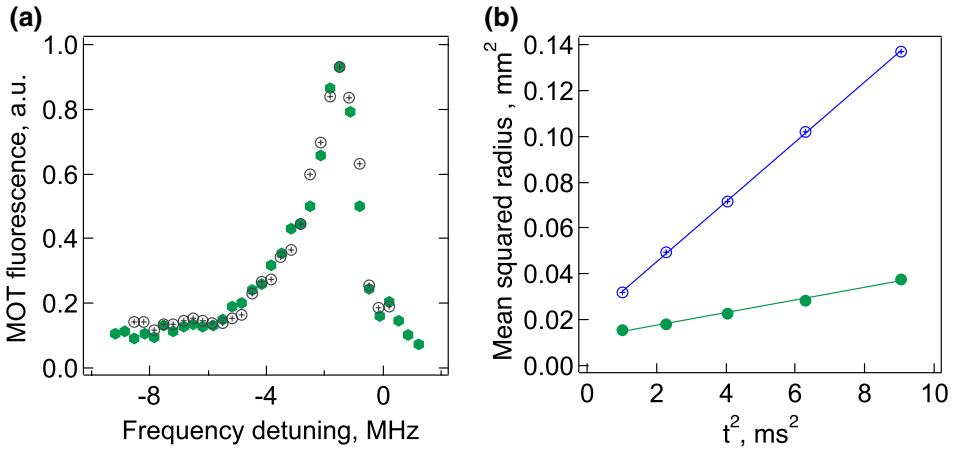

Fig. 6 **a** Cold atom fluorescence as a function of 555.8-nm frequency detuning captured 2.5 ms after release from the 398.9-nm MOT fields. The two sets of *markers* represent sweeps across the transition in opposite directions. **b** The mean-squared cloud radius versus free expansion time, t^2, for ^{171}Yb. The *upper trace* is with the 398.9-nm magneto-optical trap alone, while the *lower trace* is with the dual 398.9 and 555.8-nm MOT. The two slopes correspond to temperatures of 270 and 60 μK

light and magnetic gradient are turned off for the free expansion. While the lower trace shows the free expansion out of the dual MOT, again all electromagnetic fields, including the green light, are switched off for the release (a galvanometer driven shutter is used). The 555.8-nm intensity was $\sim 240\, I_{556}$ and the 398.9-nm light was ramped down to zero intensity over 25 ms before the release. The magnetic field gradient along the z-axis is $\sim 0.3\,\mathrm{T\,m^{-1}}$ and is held fixed before switching off. The upper trace corresponds to a temperature of 270 μK, while that of the lower is 60 μK. For ^{172}Yb, we record temperatures of ~120 μK in the dual MOT.[2] Also, the cloud size is compressed by nearly a factor of two in the dual-wavelength MOT (less evident in Fig. 6b). A Doppler broadened line corresponding to 60 μK would have a linewidth of ~230 kHz; hence, the linewidth of the 556-nm light here is constrained to a similar value (and may be less than this). These results are a validation that the injection-locking process is preserving the linewidth of the fiber laser. A further reduction in temperature may occur with better manipulation of the 555.8-nm light intensity in the MOT.

5 Conclusions

We have demonstrated a scheme of generating low-noise 555.8-nm light suitable for $^1S_0$–$^3P_1$ Yb laser cooling that uses injection locking of a semiconductor laser at 1,111.6 nm. A low-power fiber laser injection locks a 50-mW diode laser, after which second-harmonic generation in a resonant cavity is carried out. It avoids the use of high-power fiber amplifiers and crystal waveguides, both of which are costly and the latter can suffer degradation in conversion efficiency over the long term [31]. The technique should make experiments with laser-cooled Yb more accessible. We performed spectroscopy on the $^1S_0$–$^3P_1$ line in ^{172}Yb with a 555.8-nm light level of 0.01 times the saturation intensity of the line, and showed a linear dependence between the ground-state linewidth and intensity of the $^1S_0$–$^1P_1$ trapping light. Interpolating to zero intensity, we infer that the linewidth of the 555.8-nm light is less than 410 ± 90 kHz. As further confirmation of the 555.8-nm light properties, we have shown additional laser cooling of ^{171}Yb atoms in a dual 398.9 and 555.8-nm magneto-optical trap, producing temperatures well below 100 μK; hence, indicating the suitability of injection-locked 1,100–1,130-nm laser diodes as a source of sub-MHz linewidth radiation in the yellow–green spectrum.

Note added in proof Reducing the intensity of the 555.8-nm light before releasing the atoms has led to mean temperatures of 40 μK and 70 μK for ^{171}Yb and ^{172}Yb, respectively.

Acknowledgments This work was supported by the Australian Research Council (LE110100054). J.M. is supported through an ARC Future Fellowship (FT110100392) and N.K. through a Prescott Postgraduate Scholarship, UWA. We are gracious to Gary Light and Steve Osborne of the UWA Physics workshop for their technical expertise. We thank members of the ARC Centre of Excellence for Engineered Quantum Systems for their assistance, and S. Parker and E. Ivanov for the use of equipment.

[2] To be consistent with Doppler cooling theory the frequency detuning is required to be $\sim -2.5\,\Gamma_{556}$.

References

1. F.-L. Hong, J. Ishikawa, K. Sugiyama, A. Onae, H. Matsumoto, J. Ye, J. Hall, Comparison of independent optical frequency measurements using a portable iodine-stabilized Nd:YAG laser. IEEE Trans. Instrum. Meas. **52**, 240–244 (2003)
2. H.-C. Chui, S.-Y. Shaw, M.-S. Ko, Y.-W. Liu, J.-T. Shy, T. Lin, W.-Y. Cheng, R. Roussev, M. Fejer, Iodine stabilization of a diode laser in the optical communication band. Opt. Lett. **30**, 646 (2005)
3. A. Yamaguchi, S. Uetake, Y. Takahashi, A diode laser system for spectroscopy of the ultranarrow transition in ytterbium atoms. Appl. Phys. B **91**, 57–60 (2008)
4. H. Matsuura, T. Takagi, Development of a low-noise yellow–green laser using a Yb-doped double-clad fiber laser and a periodically poled $LiNbO_3$ waveguide crystal. Jpn. J. Appl. Phys. **50**, 032701 (2011)
5. N. Hinkley, J.A. Sherman, N.B. Phillips, M. Schioppo, N.D. Lemke, K. Beloy, M. Pizzocaro, C.W. Oates, A.D. Ludlow, An atomic clock with 10^{-18} instability. Science **341**, 1215–1218 (2013)
6. N.D. Lemke, A.D. Ludlow, Z.W. Barber, T.M. Fortier, S.A. Diddams, Y. Jiang, S.R. Jefferts, T.P. Heavner, T.E. Parker, C.W. Oates, Spin-½optical lattice clock. Phys. Rev. Lett. **103**, 063001 (2009)
7. M. Yasuda, H. Inaba, T. Kohnot, T. Tanabe, Y. Nakajima, K. Hosaka, D. Akamatsu, A. Onae, T. Suzuyama, M. Amemiya, F.-L. Hong, Improved absolute frequency measurement of the 171 Yb optical lattice clock towards a candidate for the redefinition of the second. Appl. Phys. Express **5**, 102401 (2012)
8. C.Y. Park, D.-H. Yu, W.-K. Lee, S.E. Park, E.B. Kim, S.K. Lee, J.W. Cho, T.H. Yoon, J. Mun, S.J. Park, T.Y. Kwon, S.-B. Lee, Absolute frequency measurement of $^1S_0(\mathrm{F}=1/2)$–$^3P_0(\mathrm{F}=1/2)$ transition of 171 Yb atoms in a one-dimensional optical lattice at KRISS. Metrologia **50**, 119 (2013)
9. M. Pizzocaro, G. Costanzo, A. Godone, F. Levi, A. Mura, M. Zoppi, D. Calonico, Realization of an ultrastable 578-nm laser for an Yb lattice clock. IEEE Trans. Ultrason. Ferroelectr. Freq. Control **59**, 426–31 (2012)
10. C. Ning, Z. Min, C. Hai-Qin, F. Su, H. Liang-Yu, Z. Xiao-Hang, G. Qi, J. Yan-Yi, B. Zhi-Yi, M. Long-Sheng, X. Xin-Ye, Clock-transition spectrum of 171Yb atoms in a one-dimensional optical lattice. Chin. Phys. B **22**, 090601 (2013)
11. T. Loftus, J. Bochinski, T. Mossberg, Simultaneous multi-isotope trapping of ytterbium. Phys. Rev. A **63**, 053401–1 (2001)
12. Y. Takasu, K. Maki, K. Komori, T. Takano, K. Honda, M. Kumakura, T. Yabuzaki, Y. Takahashi, Spin-singlet Bose–Einstein condensation of two-electron atoms. Phys. Rev. Lett. **91**, 040404 (2003)
13. T. Fukuhara, S. Sugawa, Y. Takahashi, Bose–Einstein condensation of an ytterbium isotope. Phys. Rev. A **76**, 0516041 (2007)
14. M. Okano, H. Hara, M. Muramatsu, K. Doi, S. Uetake, Y. Takasu, Y. Takahashi, Simultaneous magneto-optical trapping of lithium and ytterbium atoms towards production of ultracold polar molecules. Appl. Phys. B **98**, 691–6 (2010)
15. F. Munchow, C. Bruni, M. Madalinski, A. Gorlitz, Two-photon photoassociation spectroscopy of heteronuclear YbRb. Phys. Chem. Chem. Phys. **13**, 18734–7 (2011)
16. M. Borkowski, P. Zuchowski, R. Ciurylo, P. Julienne, D. Kedziera, L. Mentel, P. Tecmer, F. Munchow, C. Bruni, A. Gorlitz, Scattering lengths in isotopologues of the RbYb system. Phys. Rev. A **88**, 052708 (2013)
17. M. Borkowski, R. Ciurylo, P. Julienne, R. Yamazaki, H. Hara, K. Enomoto, S. Taie, S. Sugawa, Y. Takasu, Y. Takahashi, Photoassociative production of ultracold heteronuclear ytterbium molecules. Phys. Rev. A **84**, 030702 (2011)
18. Y. Takasu, Y. Takahashi, Quantum degenerate gases of ytterbium atoms. J. Phys. Soc. Jpn. **78**, 012001 (2009) (11 pp.)
19. H. Hara, Y. Takasu, Y. Yamaoka, J. Doyle, Y. Takahashi, Quantum degenerate mixtures of alkali and alkaline-earth-like atoms. Phys. Rev. Lett. **106**, 205304 (2011)
20. A. Hansen, A. Khramov, W. Dowd, A. Jamison, B. Plotkin-Swing, R. Roy, S. Gupta, Production of quantum-degenerate mixtures of ytterbium and lithium with controllable interspecies overlap. Phys. Rev. A **87**, 013615 (2013). (8 pp.)
21. S. Dorscher, A. Thobe, B. Hundt, A. Kochanke, R. Le Targat, P. Windpassinger, C. Becker, K. Sengstock, Creation of quantum-degenerate gases of ytterbium in a compact 2D-/3D-magneto-optical trap setup. Rev. Sci. Instrum. **84**, 043109 (2013)
22. S. Taie, R. Yamazaki, S. Sugawa, Y. Takahashi, An SU(6) Mott insulator of an atomic Fermi gas realized by large-spin Pomeranchuk cooling. Nat. Phys. **8**, 825 (2012)
23. G. Pagano, M. Mancini, G. Cappellini, P. Lombardi, F. Schafer, H. Hui Hu, L. Xia-Ji, J. Catani, C. Sias, M. Inguscio, L. Fallani, A one-dimensional liquid of fermions with tunable spin. Nat. Phys. **10**, 198 (2014)
24. F. Scazza, C. Hofrichter, M. Hoefer, P.C. De Groot, I. Bloch, S. Foelling, Observation of two-orbital spin-exchange interactions with ultracold SU(N)-symmetric fermions. Nat. Phys. **10**, 779 (2014)
25. F. Gerbier, J. Dalibard, Gauge fields for ultracold atoms in optical superlattices. New J. Phys. **12**, 033007 (2010)
26. H. Nonne, M. Moliner, S. Capponi, P. Lecheminant, K. Totsuka, Symmetry-protected topological phases of alkaline-earth cold fermionic atoms in one dimension. Europhys. Lett. **102**, 37008 (2013)
27. Y. Takasu, Y. Saito, Y. Takahashi, M. Borkowski, R. Ciurylo, P. Julienne, Controlled production of subradiant states of a diatomic molecule in an optical lattice. Phys. Rev. Lett. **108**, 173002 (2012)
28. V. Natarajan, Proposed search for an electric-dipole moment using laser-cooled 171Yb atoms. Eur. Phys. J. D **32**, 33–8 (2005)
29. M. Tarbutt, B. Sauer, J. Hudson, E. Hinds, Design for a fountain of YbF molecules to measure the electron's electric dipole moment. New J. Phys. **15**, 053034 (2013)
30. F. Deuretzbacher, D. Becker, J. Bjerlin, S. Reimann, L. Santos, Quantum magnetism without lattices in strongly interacting one-dimensional spinor gases. Phys. Rev. A **90**, 013611 (2014)
31. N. Chiodo, F. Du Burck, J. Hrabina, Y. Candela, J.-P. Wallerand, O. Acef, CW frequency doubling of 1029 nm radiation using single pass bulk and waveguide PPLN crystals. Opt. Commun. **311**, 239–44 (2013)
32. O. Stepanenko, E. Quillier, H. Tronche, P. Baldi, M. De Micheli, Highly confining proton exchanged waveguides on Z-Cut LiNbO3 with preserved nonlinear coefficient. IEEE Photonics Technol. Lett. **26**, 1557–60 (2014)
33. E.B. Kim, W.-K. Lee, C.Y. Park, D.-H. Yu, S.E. Park, Narrow linewidth 578 nm light generation using frequency-doubling with a waveguide PPLN pumped by an optical injection-locked diode laser. Opt. Express **18**, 10308–14 (2010)
34. M. Yasuda, T. Kohno, H. Inaba, Y. Nakajima, K. Hosaka, A. Onae, F.-L. Hong, Fiber-comb-stabilized light source at 556 nm for magneto-optical trapping of ytterbium. J. Opt. Soc. Am. B **27**, 1388–93 (2010)
35. S. Sinha, C. Langrock, M. Digonnet, M. Fejer, R. Byer, Efficient yellow-light generation by frequency doubling a narrow-linewidth 1150 nm ytterbium fiber oscillator. Opt. Lett. **31**, 347–9 (2006)

36. A. Bouchier, G. Lucas-Leclin, P. Georges, J. Maillard, Frequency doubling of an efficient continuous wave single-mode Yb-doped fiber laser at 978 nm in a periodically-poled MgO:LiNbO3 waveguide. Opt. Express **13**, 6974–6979 (2005)
37. S. Kobayashi, T. Kimura, Injection locking in AlGaAs semiconductor laser. IEEE J. Quantum Electron. **17**, 681–689 (1981)
38. N. Kostylev, E. Ivanov, M. Tobar, J.J. McFerran, Sub-Doppler cooling of ytterbium with the $^1S_0$–$^1P_1$ transition including ^{171} Yb (I $= 1/2$). J. Opt. Soc. Am. B **31**, 1614 (2014)
39. M. Cristiani, T. Valenzuela, H. Gothe, J. Eschner, Fast nondestructive temperature measurement of two-electron atoms in a magneto-optical trap. Phys. Rev. A. **81**, 063416 (2010)
40. T. Loftus, J.R. Bochinski, T.W. Mossberg, Probing magneto-optic trap dynamics through weak excitation of a coupled narrow-linewidth transition. Phys. Rev. A **61**, 061401 (2000)
41. A. Slepkov, A. Bhagwat, V. Venkataraman, P. Londero, A. Gaeta, Spectroscopy of Rb atoms in hollow-core fibers. Phys. Rev. A **81**, 053825 (2010)
42. A. Akulshin, V. Sautenkov, V. Velichansky, A. Zibrov, M. Zverkov, Power broadening of saturation absorption resonance on the D2 line of rubidium. Opt. Commun. **77**, 295–8 (1990)
43. C.N. Cohen-Tannoudji, Manipulating atoms with photons. Rev. Mod. Phys. **70**, 707 (1998)
44. H. Telle, Stabilization and modulation schemes of laser diodes for applied spectroscopy. Spectrochim. Acta Rev. **15**, 301–327 (1993)
45. S. Uetake, A. Yamaguchi, S. Kato, Y. Takahashi, High power narrow linewidth laser at 556 nm for magneto-optical trapping of ytterbium. Appl. Phys. B **92**, 33 (2008)
46. W. Kozlovsky, C. Nabors, R. Byer, Efficient second harmonic generation of a diode-laser-pumped CW Nd:YAG laser using monolithic MgO:LiNbO3 external resonant cavities. IEEE J. Quantum Electron. **24**, 913–19 (1988)
47. R. Le Targat, J. Zondy, P. Lemonde, 75%-Efficiency blue generation from an intracavity PPKTP frequency doubler. Opt. Commun. **247**, 471–81 (2005)